Unsupervised Pose Flow Learning for Pose Guided Synthesis

Haitian Zheng, *Student Member,* Lele Chen, *Student Member,* Chenliang Xu, *Member,* and Jiebo Luo, *Fellow, IEEE*

Abstract—Pose guided synthesis aims to generate a new image in an arbitrary target pose while preserving the appearance details from the source image. Existing approaches rely on either hard-coded spatial transformations or 3D body modeling. They often overlook complex non-rigid pose deformation or unmatched occluded regions, thus fail to effectively preserve appearance information. In this paper, we propose an unsupervised pose flow learning scheme that learns to transfer the appearance details from the source image. Based on such learned pose flow, we proposed GarmentNet and SynthesisNet, both of which use multi-scale feature-domain alignment for coarse-to-fine synthesis. Experiments on the DeepFashion, MVC dataset and additional real-world datasets demonstrate that our approach compares favorably with the state-of-the-art methods and generalizes to unseen poses and clothing styles.

Index Terms—Pose guided synthesis, pose correspondence, unsupervised optical flow.

I. INTRODUCTION

POSE guided synthesis aims to generate a realistic person image that preserves the appearance details of the source image given an arbitrary target pose. As a central task in virtual reality [43], online garment retail [10], and game character rendering, realistic pose guided synthesis will have a crucial impact on numerous applications.

Despite the recent successes of conditional image synthesis [11], [38], pose guided synthesis still faces many unsolved challenges. Among them, the main challenge is the complex, part-independent pose deformation, with garment, from the source pose to an arbitrary target pose. As a result, models [22], [4], [10], [29] built on the plain U-Net [32] network structure often fail to generate precise details or textures due to the lack of a robust spatial alignment component.

Recently, several approaches [34], [28], [42], [3] have been proposed to address spatial alignment. Specifically, Siarohin *et al.* [34] apply deformable skip connections for spatial alignment. However, the oversimplified affine transformation on the predefined rectangles does not necessarily capture the non-rigid deformation. Different from Siarohin *et al.*, Neverova *et al.* [28] and Wu *et al.* [42] resort to a pretrained pose estimator, DensePose [1], to perform non-rigid alignment on 3D-model. Since such model-level alignment is not capable of handling occluded regions caused by drastic pose changes, inpainting is then applied to fill the occluded region. Nonetheless, the results are usually blurry in occluded regions.

A later work [3] relies on the combination of affine transformation and thin-plate splines (TPS) transformation to perform spatial alignment. However, the TPS transformation is inflexible to model the highly non-rigid human pose deformation.

Fig. 1. Images generated by different methods. The first column contains source images while the second column contains ground truth images with target poses. We compare our results (last column) with the state-of-the-art methods (rows 3-7). The odd rows display the entire images and the even rows display the corresponding texture details. In comparison, our method clearly produces the most visually plausible and pleasing effects.

In addition, their matching module is trained on simplified synthetic transformations [31]. Therefore, the human pose deformation is not properly handled. Most recently, Li *et al.* [18] use the 3D human model [21] to generate human pose flow ground-truth for training a flow estimator. However, similar to other 3D-modeling approaches [28], [42], the issue of large occluded regions is not well addressed due to the lack of correspondence. Moreover, the 3D human modeling is computationally expensive, and it is not always precise on loose clothes, as 3D human modeling focus on body reconstruction rather than the clothes surface reconstruction.

In this paper, we present i) a novel unsupervised pose flow learning scheme (Stage-I) to tackle the pose guided transfer task. Next, we propose ii) a coarse-to-fine garment-to-image synthesis pipeline (Stage-II) using feature domain alignment based on the learned flow. Without using affine or TPS transformation [34], [3] or resorting to explicit 3D human modeling [28], [42], [18] to extract correspondence, our method utilizes learned pose flow to capture the complex pose deformation. To address the issue of occlusion caused by drastic pose changes, we propose an unsupervised pose flow learning scheme that learns to transfers appearance to occluded regions. In contrast to [18], our approach avoids the computationally inefficient flow ground-truth generation step.

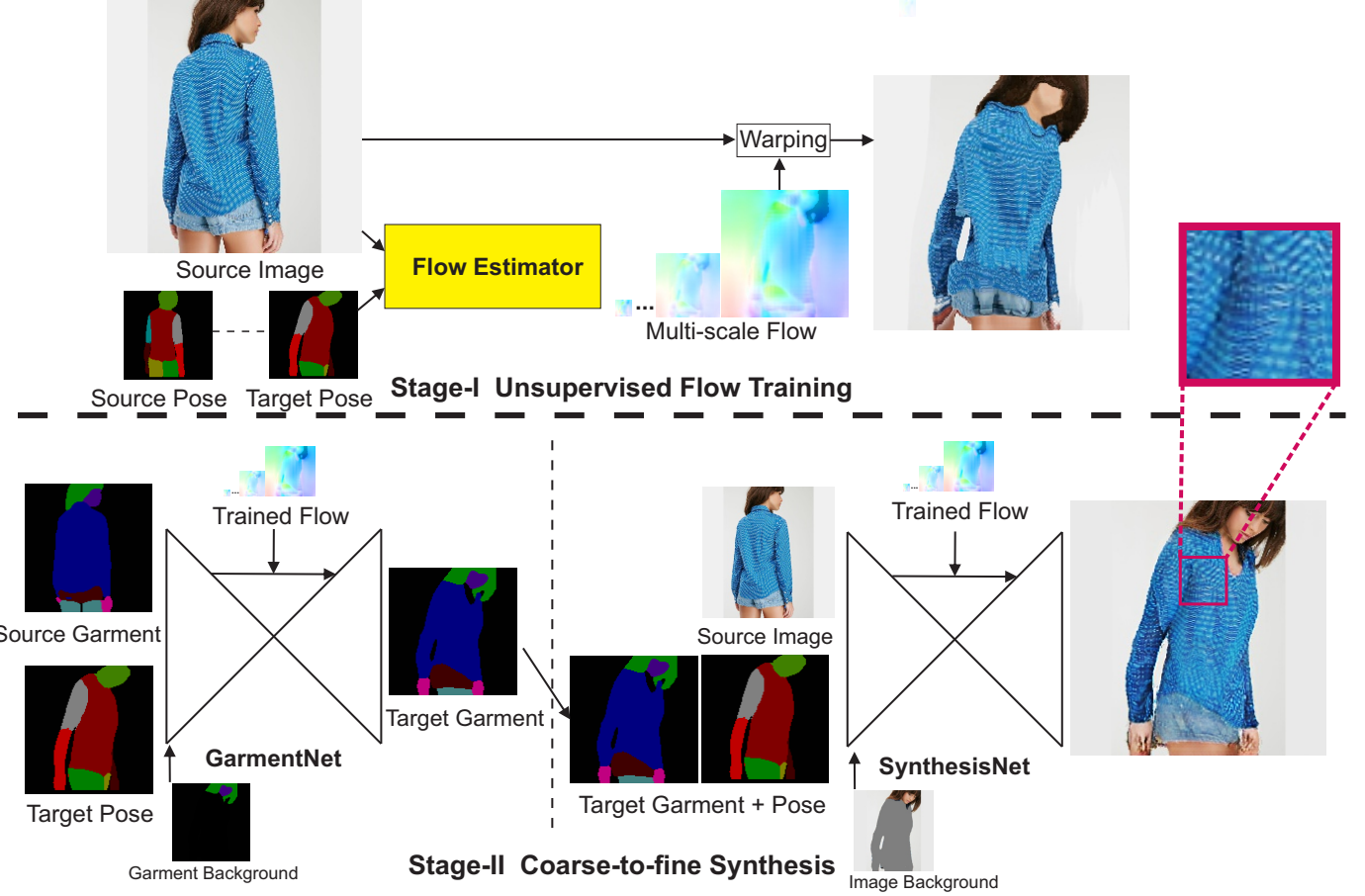To enable such an unsupervised pose flow training scheme,

Fig. 2. Our two-stage framework for pose-guided person image synthesis. In stage-I, a flow estimator is trained using our proposed texture-preserving objective. In stage-II, GarmentNet and SynthesisNet use the trained flow estimator to sequentially estimate garment parsing and image output, following a course-to-fine pipeline.

we propose in Stage-I a novel texture preserving objective to improve the quality of the learned flow, which is shown to be crucial for the pose-guided synthesis task. We also propose augmentation-based self-supervision to stabilize the flow training. Based on the learned pose flow, we proposed in Stage-II a coarse-to-fine garment-to-image synthesis pipeline using our proposed GarmentNet and SynthesisNet. GarmentNet and SynthesisNet share a unified network structure, which utilizes the learned pose flow for multi-scale feature domain warping. Furthermore, we propose a novel gated multiplicative attention module for misalignment-aware synthesis.

Finally, to synthesize more realistic images, we design masking layers in GarmentNet and SynthesisNet to preserve the target image background and person identity for realistic synthesis. Furthermore, we use DensePose parsing [1] instead of person keypoints as pose inputs. DensePose parsing contains body segmentation and mesh coordinates, which provide richer information for realistic pose-guided synthesis.

Our main contributions are three-fold:

- We propose an unsupervised pose flow learning scheme for pose-guided synthesis. Our scheme adaptively learns to transfer appearance from target images. To enable such a learning scheme, a novel texture preserving objective

and an augmentation-based self-supervision strategy are proposed, which improve the quality of the transferred appearance.
- We propose a coarse-to-fine synthesis pipeline based on GarmentNet and SynthesisNet. GarmentNet and SynthesisNet are based on the learned pose flow for multi-scale feature domain alignment. Furthermore, a novel gated multiplicative attention module is proposed to address the misalignment issue.
- To facilitate more realistic image synthesis, we design masking layers that preserve target identities and background information. Furthermore, we use DensePose parsing as pose representation, which provides richer pose details for pose-guided synthesis.

The remainder of the paper is organized as follows. Sec. II introduces related work on (pose guided) image synthesis and optical flow learning. The proposed approach is detailed in Sec. III. Experiments are described in Sec. IV. Sec. V concludes the paper.

II. RELATED WORK

A. Image synthesis

Generative Adversarial Network (GAN) [8] has been widely used for image synthesis tasks. Conditional GAN [26] aims to

synthesize an image from an given conditional input content. Based on conditional GAN, Isola *et al.* propose Pix2Pix [11] for image style transfer tasks. Later on, many techniques have been proposed to improve both the synthesis quality and resolution of the generated images. Specifically, Johnson *et al.* [14] use feature-level distance on the VGG network [35] to measure the perceptual similarities. The Gram matrix loss [6] is proposed by Gatys *et al.* for texture synthesis. To improve the image synthesis resolution, Zhang *et al.* [44] propose a two-stage network for generating images from coarse to fine scales. PatchGAN discriminator [17] is used by Li *et al.* to penalize unrealistic patches. Wang *et al.* [38] and Chen *et al.* [2] propose new generator structures for realistic image synthesis. In addition, techniques such as Wasserstein distance [9] and Spectral Normalization [27] are proposed to stabilize GAN training. Those approaches have improved the synthesized image quality. However, these approaches are limited to spatial deformation as their networks are built on local convolution. In this work, we present a flow-based approach to address the spatial alignment problem in pose-guided synthesis.

B. Pose Guide Synthesis

Ma *et al.* [22] use the source image and target pose landmarks as the conditional input and the UNet [32] structure for pose guided synthesis. Later, Siarohin *et al.* [34] utilize skip connections with hard-coded part-level affine transformation to transform feature maps for new pose image synthesis. Dong *et al.* [3] use the thin-plate spline (TPS) transform trained on synthetic transformations [31] to warp the source domain content. Additionally, Han *et al.* [10] and Wang *et al.* [37] use the TPS transformer for virtual try-on. To handle pose deformations, Neverova *et al.* [28] use DensePose [1] to transfer appearance patterns and utilize in-painting to fill occluded regions. In addition, pose guided synthesis is formulated as a pose-appearance disentanglement problem. Specifically, Esser *et al.* [4] use variational autoencoder [16] to capture the latent space of pose and appearance for appearance manipulation under given poses. Ma *et al.* [23] learn disentangled pose-appearance representation using a multi-branch encoding and decoding scheme. However, the plain UNet structure [22], [4], predefined transformation [34], [28] or TPS transformer [3], [37] are insufficient for handling the complex human pose deformation and occlusion caused by drastic pose changes. Recently, Li *et al.* [18] uses 3D human model [21] to correspondence annotation, then fit a flow estimator to speed up inference. However, generating the correspondence supervision is computationally exhausted. Furthermore the ground-truth correspondence cannot effectively transfer appearance to occluded regions. In contrast, our unsupervised flow-training scheme learns to transfer appearance under complex pose deformation and occlusion without using explicit correspondence annotation.

C. Unsupervised Optical Flow Learning

Recently, several approaches have been proposed to learn optical flow in the absence of the ground-truth annotation. Specifically, Jason *et al.* [13] optimize a predictive model using a combination of photometric loss and smoothness. Meister *et al.* [25] utilize left-right consistency to filter out occluded regions. Wang *et al.* [39] further propose an occlusion-aware objective function for unsupervised flow learning. Different from these works, we focus on learning a flow that better preserves the appearance information. Furthermore, our optical flow is estimated using only the source image and pose information.

III. APPROACH

In this section, we present an unsupervised flow-based approach to the pose-guided synthesis task. To this end, we adopt a two-stage pipeline, as illustrated in Fig. 2. In Stage-I, a flow estimator is unsupervisedly trained using our proposed texture-preserving objective. In Stage-II, we present GarmentNet and SynthesisNet to sequentially generate garment parsing and image output, using the flow obtained from the previous stage.

In Sec. III-A, we first define the notation that are required by our model. In Sec. III-B, we propose our unsupervised texture-preserving objective and other details for training flow estimator for pose-guided alignment. In Sec. III-C, we propose GarmentNet and SynthesisNet to respectively estimate garment parsing and image output.

A. Notations

Given a pair of images I_s and I_t from the source and target domains respectively, pose-guided synthesis aims to generate a image $\hat{I}_t$ that preserves the appearance of I_s and the pose of I_t. To this end, we respectively generate *pose representation* P_s, P_t and *garment parsing* G_s, G_t from I_s and I_t, to capture useful information from the source and target domains. In addition, we extract image residue I_t^r from I_t and garment residues G_t^r from garment G_t, in the hope to capture target identity (i.e., face, hair, and background regions). Fig. 3 illustrates (P_s, P_t), (G_s, G_t), (I_s, I_t) and residues (I_t^r, G_t^r). In fact, P_t, G_t and I_t form an hierarchical structure that gradually provide richer information of the target person. We leverage this hierarchical structure in Sec. III-C to design our coarse-to-fine synthesis pipeline. We note that during training, I_s and I_t are from the same outfit of the same person. In testing phase, however, I_s and I_t can be arbitrary person with arbitrary outfits.

To be more specific, the pose representations P_s and P_t are the concatenation of the one-hot pose parsing and the mesh coordinate map from Densepose [1]. Likewise, the garment representations G_s and G_t are the one-hot garment parsing generated using the method by Gong *et al.* [7]. The image residue r_t^i are generated by first removing person region from I_t then perform inpainting []. Then, hair and face regions are appended on the inpainted results [1]. Finally, garment residue r_t^g are generated by setting values of one-hot parsing G_t to 0 for background, face and hair channels.

Although our approach can adapt key-point heat maps as an alternative human pose representation, we argue that sparse

---

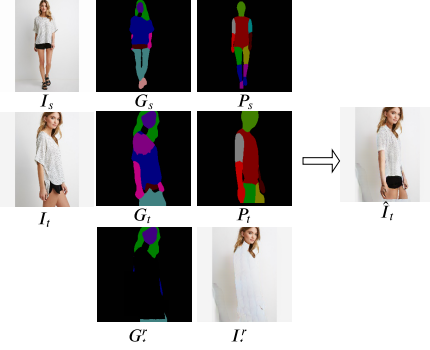[1] We use the garment parsing G_t to generate the regions of human body, hair and face.

Fig. 3. Notation illustrations for the required data for training and testing. We use subscripts s and t to represent source and target domains, respectively. The notions of I, G and P represent images, garment parsing and pose representation, respectively. (I_t^r, G_t^r) denote image residue and garment residue from the target person. The output of our approach is denoted by $\hat{I}_t$. Please refer to Sec. III-A for more details.
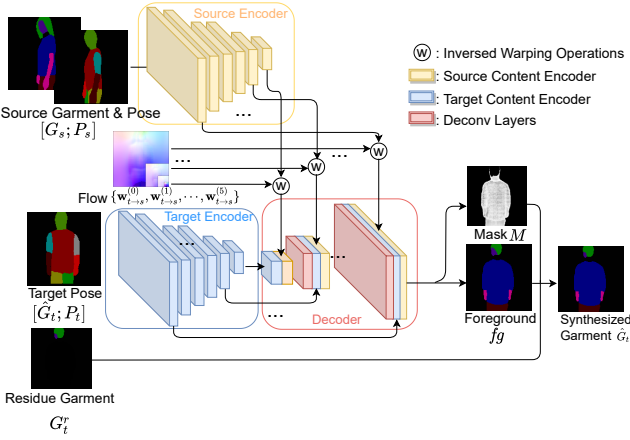

Fig. 4. The network structure of GarmentNet. Given the generated flow from Stage-I, GarmentNet encodes information from the source and target domains using a Source Domain Encoder (yellow) and a Target Domain Encoder (blue), respectively. After warping-based alignment, the source domain features are aggregated with the target domain features at multiple scales by our Decoder (red). Finally, the generated foreground is alpha-blended with the residue garment to synthesize garment parsing. In testing stage, the source and target image are from different persons.

key-points do not provide sufficient pose information for accurate person image generation. By contrast, DensePose parsing and mesh coordinates provide dense, pseudo-3D information, which is informative to represent pose detail.

B. Stage-I: Unsupervised Texture Preserving Flow

With the extracted pose representations P_s and P_t, we present an unsupervised flow training scheme to generate adaptive, texture-preserving alignment without resorting to the computationally inefficient SMPL model [21] or oversimplified affine [34] or TPS transformation [37], [3].

As shown in Fig. 2, our flow estimator takes the source image, pose and target pose as inputs to generate multi-scale flow-fields to indicate the pose deformation. Formally, let $\text{Flow}(\cdot, \cdot)$ denote our flow estimator, which takes $[I_s; P_s]$ and P_t from source and target domains as inputs and outputs flow

fields at multiple scales:

$$\{\mathbf{w}_{t \to s}^{(0)}, \mathbf{w}_{t \to s}^{(1)}, \cdots, \mathbf{w}_{t \to s}^{(5)}\} = \text{Flow}([I_s; P_s], P_t). \quad (1)$$

where notation $\mathbf{w}_{t \to s}^{(l)}$ denotes flow field from the target image to the source images at scale $l \in \{0, \cdots, 5\}$.

We employ FlowNetS [5] as the baseline structure to implement $\text{Flow}([I_s; P_s], P_t)$. Note that, unlike a normal flow estimator, $\text{Flow}(\cdot, \cdot)$ leverages pose information for flow estimation. Meanwhile, we have also modified FlowNetS to improve the flow-field definition and to reduce memory usage. Please refer to Appendix A for more details.

Unsupervised flow training on natural images has been explored in several recent works. These approaches mainly rely on the photometric loss [13]

$$\mathcal{L}_p(I_s, I_t, \mathbf{w}_{t \to s}^{(0)}) = \left\| \rho \left(I_t - \text{warp}(I_s; \mathbf{w}_{t \to s}^{(0)}) \right) \right\|_1 \quad (2)$$

to measure the difference between the target image and the inversely warped source image using the predicted flow. Here, $\text{warp}(\cdot; \cdot)$ denotes the inverse warping operation [12] and $\rho(x) = (x^2 + \epsilon^2)^\alpha$ is a robust loss function [36]. Furthermore, total variation-based (TV) spatial smoothness loss is also utilized to regularize the flow prediction [30]:

$$\mathcal{L}_{TV}(\mathbf{w}_{t \to s}^{(l)}) = \left\| \frac{\partial}{\partial x} \mathbf{w}_{t \to s}^{(l)} \right\|_1 + \left\| \frac{\partial}{\partial y} \mathbf{w}_{t \to s}^{(l)} \right\|_1. \quad (3)$$

Due to the complexity of person images and the large displacement from source pose to target pose, the warping-based photometric term is highly non-convex. As as result, the gradient descendent training with the naive photometric loss and spatial smoothness loss will lead to difficulty in convergence. To solve this issue, we use multi-scale strategy, where photometric losses and spatial smoothness losses summed at multiple scales $l \in \{0, \cdots, 5\}$.

In our experiment, we found that the multi-scale training will still suffer from damaged local textures for the warped images $\text{warp}(I_s; \mathbf{w}_{t \to s}^{(0)})$, and the learned flow fails to transfer realistic details from source images (see Fig. 8 for details). We attribute this deficiency to the poor ability of $\mathcal{L}_p$ and $\mathcal{L}_{TV}$ in preserving the high-frequency texture. In order to preserve realistic details and textures for better pose-guided synthesis, we propose a texture-preserving objective $\mathcal{L}_{texture}^{(l)}$ that enforces texture similarity between the I_t and $\text{warp}(I_s; \mathbf{w}_{t \to s}^{(0)})$ at scale l:

$$\begin{aligned} &\mathcal{L}_{texture}^{(l)}(I_t, I_s, \mathbf{w}_{t \to s}^{(0)}) \\ &= \left\| \mathbf{G}\left(\mathbf{f}_{vgg}^{(l)}(I_t) \right) - \mathbf{G}\left(\mathbf{f}_{vgg}^{(l)}(\text{warp}(I_s; \mathbf{w}_{t \to s}^{(0)})) \right) \right\|_1, \end{aligned} \quad (4)$$

where $\mathbf{f}_{vgg}^{(l)}(\cdot)$ represents the l'th VGG [35] feature map from layer {relu1_2, relu2_2, relu3_2, relu4_2, relu4_3} of the given input image, and $\mathbf{G}(\cdot)$ denotes the Gram matrix [6] to capture the second-order statistic of the given feature map. Although the objective $\mathcal{L}_{texture}^{(l)}$ is widely used in style transfer tasks, we are the first to show that the texture loss is crucial for learning a reasonable flow estimator for pose-guided synthesis tasks (see Fig. 8 for details).

Finally, we use a multi-scale version of the three losses, which are then weighted summed to compute the final loss.
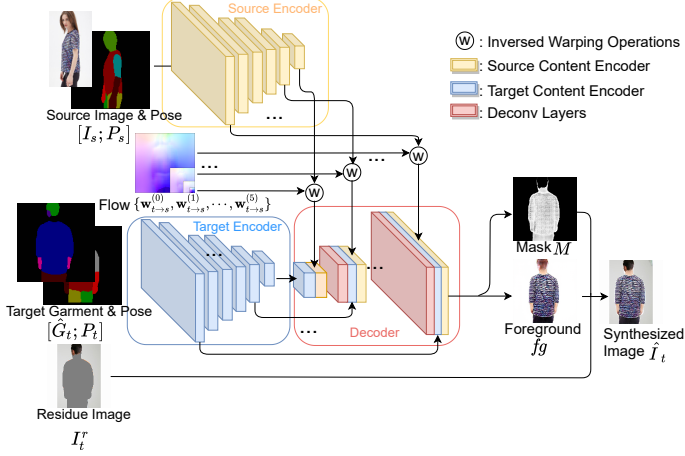
Fig. 5. The network structure of SynthesisNet. Given the generated flow from Stage-I and the synthesized garment parsing, GarmentNet encodes information from the source and target domains using a Source Domain Encoder (yellow) and a Target Domain Encoder (blue), respectively. After warping-based alignment, the source domain features are aggregated with the target domain features at multiple scales by the Decoder (red). Finally, the generated foreground is alpha blended with the residue image to synthesize image output. In testing stage, the source and target image are from different persons.

Let $I_s^{(l)}$ and $I_t^{(l)}$ denote the resized images of I_s and I_t at scale $l \in \{0, \cdots, 5\}$, the overall objective is given by:

$$
\begin{aligned}
\mathcal{L}_{StageI} \\
= \sum_{l=0}^{5} s_l (\mathcal{L}_p(I_s^{(l)}, I_t^{(l)}, \mathbf{w}_{t \to s}^{(l)}) \\
+ \beta_l \mathcal{L}_{texture}^{(l)}(I_t, I_s, \mathbf{w}_{t \to s}^{(0)}) \\
+ \gamma_l \mathcal{L}_{TV}(\mathbf{w}_{t \to s}^{(l)})),
\end{aligned}
\tag{5}
$$

with $(s_0, s_1, s_2, s_3, s_4) = (1, 1, 0.5, 0.25, 0.125)$, $(\beta_0, \beta_1, \beta_2, \beta_3, \beta_4) = (0.002, 0.002, 0.002, 0.002, 0)$, $(\gamma_0, \gamma_1, \gamma_2, \gamma_3, \gamma_4) = (0.1, 0.1, 0.1, 0.1, 0)$.

To further stabilize the training, an augmentation-based self-supervision is employed to regularize the learned flow. Specifically, let $\text{Aug}(\cdot, \theta)$ denote an augmentation transformation based on cropping, affine transformation and flipping with a random control parameter θ, the augmented source pose and source image are treated as target pose and target image, respectively. More precisely, we use the following update rules to transform the original data before one iteration of flow estimator training:

$$
\begin{aligned}
\epsilon &\sim U(0, 1), \\
P_t &\leftarrow \text{Aug}(P_s, \theta), \text{if } \epsilon < 0.25 \\
I_t &\leftarrow \text{Aug}(I_s, \theta), \text{if } \epsilon < 0.25.
\end{aligned}
\tag{6}
$$

During training, 25% percent of the training samples are first generated using such a synthetic random transformation to help the flow estimator to learn from simple transformations.

C. Stage-II: Coarse-to-Fine Synthesis

Based on the learned flow estimator in Stage-I, we propose GarmentNet and SynthesisNet to sequentially synthesize

garment parsing and image output following a coarse-to-fine pipeline (Fig. 2 bottom). As illustrated in Fig. 4 and Fig. 5, GarmentNet and SynthesisNet share a unified network structure, which utilize the learned flow in stage-I for feature alignment. Afterwards, U-Net decoder serves to fuse information from both the source and target domains. On top of the decoder, an alpha blending layer is applied to preserve background information and to generate final outputs.

Formally, GarmentNet utilizes $[G_s, P_s]$ to encode source domain information, P_t to encode target domain information, $\{\mathbf{w}_{t \to s}^{(0)}, \mathbf{w}_{t \to s}^{(1)}, \cdots, \mathbf{w}_{t \to s}^{(5)}\}$ from stage-I for alignment, and G_t^r to keep the shape of target hair and face. The notation $[\cdot, \cdot]$ denotes channal-wise concatenation. The output target garment of GarmentNet is denoted by $\hat{G}_t$:

$$
\begin{aligned}
\hat{G}_t = \text{GarmentNet}([G_s, P_s], P_t, \\
\{\mathbf{w}_{t \to s}^{(0)}, \mathbf{w}_{t \to s}^{(1)}, \cdots, \mathbf{w}_{t \to s}^{(5)}\}, I_t^r).
\end{aligned}
\tag{7}
$$

Similarly, SynthesisNet (see Eq. 8) utilizes $[I_s, P_s]$ to encode source domain information, $[\hat{G}_t, P_t]$ to encode target domain information, $\{\mathbf{w}_{t \to s}^{(0)}, \mathbf{w}_{t \to s}^{(1)}, \cdots, \mathbf{w}_{t \to s}^{(5)}\}$ from stage-I for alignment, and I_t^r to keep the background, hair and face of target image. The output of SynthesisNet is the synthesized image $\hat{I}_t$:

$$
\begin{aligned}
\hat{I}_t = \text{SynthesisNet}([I_s, P_s], [\hat{G}_t, P_t], \\
\{\mathbf{w}_{t \to s}^{(0)}, \mathbf{w}_{t \to s}^{(1)}, \cdots, \mathbf{w}_{t \to s}^{(5)}\}, I_t^r).
\end{aligned}
\tag{8}
$$

Since the two networks share the similar inputs format and network structure, we elaborate the shared network structure below.

Network Structure As shown in Fig. 4 and 5, our model relies on a source encoder $\text{Enc}_s(\cdot)$ and a target encoder $\text{Enc}_t(\cdot)$ to respectively generate multi-scale feature maps from source and target domains inputs IN_s, IN_t:

$$
\begin{aligned}
\{\mathbf{f}_s^{(0)}, \cdots, \mathbf{f}_s^{(5)}\} = \text{Enc}_s(IN_s), \\
\{\mathbf{f}_t^{(0)}, \cdots, \mathbf{f}_t^{(5)}\} = \text{Enc}_t(IN_t).
\end{aligned}
\tag{9}
$$

For GarmentNet, inputs are set to $IN_s = [G_s, P_s], IN_t = P_t$. For SynthesisNet, inputs are set to $IN_s = [I_s, P_s], IN_t = [\hat{G}_t, P_t]$.

We use six stacked strided convolutional layers to implement $\text{Enc}_t(\cdot)$ and six stacked strided convolutional layers following seven residue blocks to implement $\text{Enc}_s(\cdot)$. The additional residue blocks serve to increase feature representation capacity.

To perform spatial alignment, the source domain features $\mathbf{f}^{(l)}$ at all scales $l \in \{0, \cdots, 5\}$ are inversely warped [12] to target domain using $\mathbf{f}_s^{(l)}$ and $\mathbf{w}_{t \to s}^{(l)}$ for layers $l \in \{1, \cdots, 5\}$, formally:

$$
\mathbf{f}_{s \to t}^{(l)} = \text{warp}(\mathbf{f}_s^{(l)}; \mathbf{w}_{t \to s}^{(l)}).
\tag{10}
$$

After spatial alignment, a U-Net fusion decoder is used for feature aggregation. However, instead of directly concatenating feature maps for aggregation, we propose a gated multiplicative attention module to filter the misaligned source

domain features. Specifically, the gated multiplicative attention filtering at scale l is defined as:

$$\mathbf{f}_{s \to t}^{(l)\prime} = \mathbf{f}_{s \to t}^{(l)} \odot \sigma(\mathbf{f}_{s \to t}^{(l)\top} \mathbf{W}^{(l)} \mathbf{f}_{t}^{(l)}), \tag{11}$$

where $\sigma(\cdot)$ represents the sigmoid function, $\odot$ represents element-wise multiplication and $\mathbf{W}^{(l)}$ is a learnable matrix that measures dot product similarities between $\mathbf{f}_s^{(l)}$ and $\mathbf{f}_t^{(l)}$ on to-be-learned linear space. The gated multiplicative attention filtering can be efficiently implemented on the 2-D feature maps using 1×1 convolution, element-wise multiplication and summation. Please refer to Appendix B for details. Building on top of the gated multiplicative attention filtering operation, our decoder uses the following equations to generate the aggregated feature maps $\mathbf{f}_{dec}^{(l)}$:

$$\begin{aligned} \mathbf{f}_{dec}^{(0)} &= \mathrm{Deconv}([\mathbf{f}_{s \to t}^{(0)\prime}; \mathbf{f}_{t}^{(0)}]), \\ \mathbf{f}_{dec}^{(l)} &= \mathrm{Deconv}([\mathbf{f}_{dec}^{(l-1)}; \mathbf{f}_{s \to t}^{(l)\prime}; \mathbf{f}_{t}^{(l)}]), l \in \{1, \cdots, 5\}. \end{aligned} \tag{12}$$

Afterwards, our network simultaneously generates foreground content fg along with a mask M that ranges from 0 to 1 to avoid changing the residue content of the target r_t. Specifically, $\mathbf{f}_{dec}^{(5)}$ is passed to two independent convolutional layers to respectively generate foreground content fg and a corresponding foreground mask M:

$$\begin{aligned} fg &= \mathrm{Conv}(\mathbf{f}_{dec}^{(5)}), \\ M &= \mathrm{Conv}(\mathbf{f}_{dec}^{(5)}). \end{aligned} \tag{13}$$

Finally, the output content out is generated by alpha-blending the foreground content fg with the residue content r:

$$out = M \odot fg + (1 - M) \odot r. \tag{14}$$

For GarmentNet, softmax function is applied after out to generate the garment parsing, i.e. $\hat{G}_s = \mathrm{softmax}(out)$. For SynthesisNet, tanh function is applied after out to generate the normalized image, i.e. $\hat{I}_s = \tanh(out)$.

Training Objective For GarmentNet training, we use the cross entropy loss between the target garment G_t and prediction $\hat{G}_t$:

$$\mathcal{L}_{\mathrm{GarmentNet}} = -\sum_{i,j} \sum_{n} (G_t)_{i,j,n} \log((\hat{G}_t)_{i,j,n}), \tag{15}$$

where i, j enumerate pixel positions and n enumerates channals of garment parsing.

For SynthesisNet training, we use a combination of ℓ_1 pixel domain loss, VGG feature loss, texture loss, and GAN loss. The training objective is represented as:

$$\begin{aligned} \mathcal{L}_{\mathrm{SynthesisNet}} = &\lambda_1 \mathcal{L}_1 + \lambda_2 \mathcal{L}_{\mathrm{VGG}} \\ &+ \lambda_3 \mathcal{L}_{\mathrm{texture}} + \lambda_4 \mathcal{L}_{\mathrm{GAN}}, \end{aligned} \tag{16}$$

where $\mathcal{L}_1 = \left\| \hat{I}_t - I_t \right\|_1$ computes the ℓ_1 differences between the synthesized image and the ground-truth, $\mathcal{L}_{\mathrm{VGG}} = \left\| \mathbf{f}_{\mathrm{VGG}}(\hat{I}_t) - \mathbf{f}_{\mathrm{VGG}}(I_t) \right\|_1$ computes feature map differences on the `relu4_2` layer of the VGG network of the two image. Similar to Eq. 4, $\mathcal{L}_{\mathrm{texture}} = \left\| \mathbf{G}\left(\mathbf{f}_{\mathrm{VGG}}(\hat{I}_t)\right) - \mathbf{G}\left(\mathbf{f}_{\mathrm{VGG}}(I_t)\right) \right\|_1$ (Eq. 4) computes the texture-level differences of the two

images, and $\mathcal{L}_{\mathrm{GAN}} = \left(D(I_t) - 1\right)^2 + D(\hat{I}_t)^2$ measures how well the synthetic image can fool a trained discriminator $D(\cdot)$. Similar to CycleGAN [46], we use least-square distance [24] rather than negative log likelihood to compute the $\mathcal{L}_{\mathrm{GAN}}$, whereas the discriminator is implemented using the PatchGAN architecture [11] with spectrum normalization [27]. The hyper-parameters $\lambda_1, \lambda_2, \lambda_3, \lambda_4$ are set to $\lambda_1 = 1.0, \lambda_2 = 0.1, \lambda_3 = 0.002, \lambda_4 = 0.5$ respectively in our experiments.

Additionally, we use a similar augmentation-based self-supervision strategy as described in Sec. III-B to regularize SynthesisNet. During training, 25% percent of the source domain samples come from the augmented target domain samples to help SynthesisNet to learn from simple tasks first.

IV. EXPERIMENTS

A. Dataset

We train and evaluate our method on the DeepFashion [20] dataset, which contains 52,712 person images of sizes 256×256. Images that only contain trousers are removed using DensePose [1], resulting in 40,906 valid images. We randomly divide the dataset into 68,944 training pairs and 1,000 testing pairs. Additionally, we evaluate our DeepFashion trained model on other datasets to understand how well our model can generalize to unseen poses, clothing styles or background.

As detailed in Section III-A, pose representation are generated using DensePose, while garment representation are generated using the method of [7]. Finally, we additionally uses keypoint heatmap [22] as pose representation to test our algorithm.

B. Implementation Details

In Stage-I and Stage-II, we set the learning rate to 0.0001 for the flow estimator and the generator. Following [27], the learning rate for the discriminator is 0.0004. We adopt Adam [15] optimizer ($\beta_1 = 0.9$ and $\beta_2 = 0.999$) in all experiments. Random cropping, affine transformation and flipping are used to augment data. The flow estimator, GarmentNet and SynthesisNet are trained for 20, 20 and 40 epochs, respectively.

Since our approach can adopt keypoint heatmap [22] as pose representation by simply altering P_s, P_t, we additionally train our model using the key point representation while maintaining other inputs unchanged.

C. Quantitative Evaluation

To quantitatively evaluate the synthesis results, low-level metrics like Structural Similarity (SSIM) [40], Multi-scale Structural Similarity (MS-SSIM) [41] and perceptual-level metrices like Inception Score (IS) [33] and the Perceptual Image Patch Similarity Distance (LPIPS) [45] are measured on different approaches, including PG2 [22], BodyROI [23], Vunet [4], DSCF [34], Soft-gated GAN (Soft-gate) [3] and Intrinsic Flow (IF) [18]. For LPIPS, we use the linearly calibrated Alex model, please refer to [45] for details. Since our approach relies on the background information, we report the masked version of all the metrices for fair comparisons. The masks are generated by running [7] to exclude background,

TABLE I

QUANTITATIVE COMPARISON OF DIFFERENT METHODS IN TERMS OF BOTH THE MASKED SSIM/MSSSIM/INCEPTION SCORE (IS) AND THE LEARNED PERCEPTUAL IMAGE PATCH SIMILARITY (LPIPS) AT 256 × 256 AND 128 × 128 RESOLUTION. HIGHER SCORES ARE BETTER FOR METRICS WITH UPARROW (↑), AND VICE VERSA.

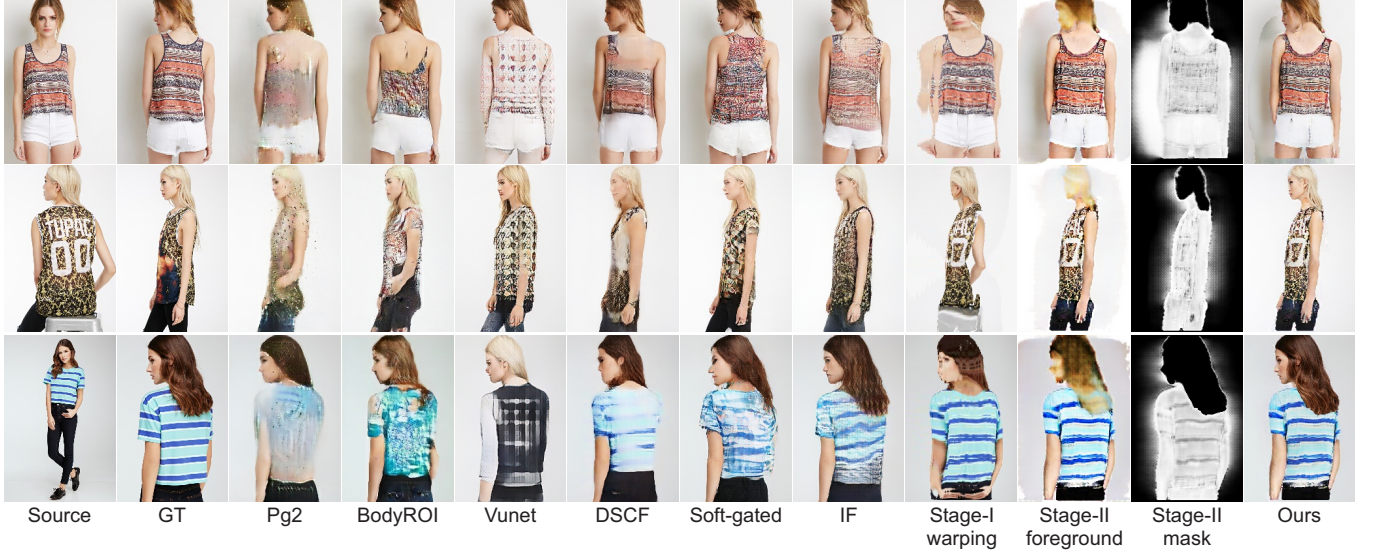| Methods	SSIM-128↑	msSSIM-128↑	SSIM↑	msSSIM↑	IS-128↑	IS↑	LPIPS↓	LPIPS-128↓
PG2 [22]	0.864	0.911	0.857	0.891	3.455 ± 0.226	4.266 ± 0.371	0.192	0.190
BodyROI7 [23]	0.842	0.882	0.837	0.865	3.282 ± 0.173	3.855 ± 0.158	0.193	0.201
DSCF [34]	0.856	0.902	0.851	0.884	3.458 ± 0.198	4.226 ± 0.326	0.159	0.157
Vunet [4]	0.822	0.830	0.827	0.827	3.424 ± 0.143	4.176 ± 0.320	0.226	0.258
Soft-gate [3]	0.860	0.908	0.853	0.888	3.270 ± 0.219	3.868 ± 0.387	0.140	0.135
IF [18]	**0.877**	**0.926**	**0.865**	**0.906**	3.262 ± 0.293	3.809 ± 0.360	0.128	0.128
Ours	0.854	0.905	0.848	0.884	3.540 ± 0.294	4.197 ± 0.291	**0.124**	**0.124**
Ours-kp	0.831	0.870	0.831	0.852	**3.646 ± 0.285**	**4.295 ± 0.296**	0.163	0.169

Fig. 6. Comparison with the state-of-the-art approaches. The last four columns depict the warped source image, fore ground prediction in stage-II, mask prediction in stage-II, and our final output. In comparison, our method clearly produces the most visually plausible and pleasing effects.
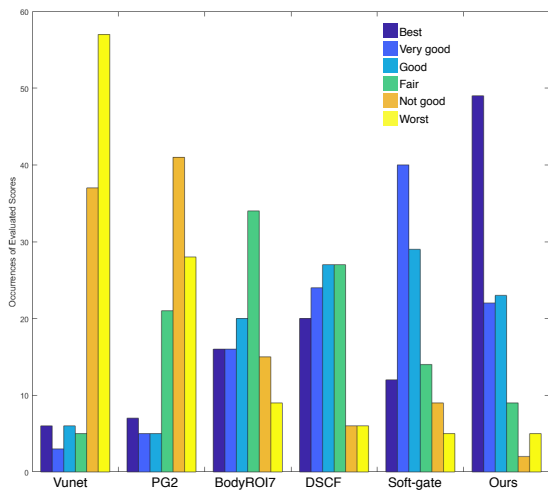

Fig. 7. Subjective quality assessment of different algorithms. For each algorithm, the bar depicts the number of occurrences of scores, while blue to yellow colors represent the scores from the best to the worst.

hair, and face region. We additionally test all the metrics at resolution 128 × 128 to measure similarities at a global scale.

From Table I, our method (*ours*) substantially outperforms the remaining methods in IS-based measurements and LPIPS distances, as our texture-preserving flow is able to preserve texture patterns form source images. In terms of the low-level SSIM-based measurements, our method achieves competitive performance in comparison with the other approaches. When trained using keypoint heatmap (*ours-kp*), we observe similar high IS scores for both models and better LPIPS scores for our model. It suggests both models (*ours* and *ours-kp*) preserve realistic texture. However, with the help of the DensePose pose representation, our model (*ours*) generates better global shape.

D. Qualitative Evaluation

We conduct a subjective assessment to evaluate our method qualitatively. Specifically, we ask 15 subjects to rank image qualities among the 6 algorithms ([4], [22], [23], [34], [3] and ours). The subjects are instructed to rank the six images, based on the realism of the generated garments as well as global garment structures. The subjects are then asked to provide a score from 1 to 6 for each image, representing best quality to worst quality, respectively. We plot the ranking

histogram of different algorithms in Fig. 7. From the figure, our method is most frequently chosen as the best due to structurally consistent texture. DSCF [34] achieves the second place due to its ability to maintain texture structure from the source image using rigid transformations. The qualitative results of different approaches as well as the warped source image and foreground/mask prediction from stage-II are shown in Fig. 6. It can be noticed that the existed approaches generate blurry results or incorrect textures. By contrast, our method can preserve texture details from source images. Notably, our approach generates better warping results in comparison with IF, especially under large pose changes.

E. Ablation Study

Unsupervised Flow Training   To evaluate the effectiveness of each component in the unsupervised flow training scheme, we separately train three variants of the proposed flow estimators: i) *w/o multi-scale*, only computing loss at the finest scale, ii) *w/o texture*, removing texture loss $\mathcal{L}_{texture}$, and iii) *w/o semi*, removing the augmentation-based self supervision. Table II compares the three models with our full model by computing the SSIM, IS, and LPIPS-based scores of the inversely warped images using the trained flow at the finest scale. The inversely warped image is also visualized in Fig.8. It is observed that our full model outperforms *w/o semi* and *w/o multi-scale* in terms of LPIPS scores. It is consistent with the visualization from Fig. 8, showing that our full model can generate flow with more visually plausible and pleasing details. The *w/o multi-scale* performs well in IS scores, and it is possibly because *w/o multi-scale* tends to retain the realistic original source image. However, *w/o multi-scale* does not preserve the semantics of the target pose. In terms of SSIM-based measurement, the full flow training scheme achieves the best ms-SSIM scores, suggesting that the full model is better at preserving global structures.

SynthesisNet Design   To evaluate the effectiveness of different components in training SynthesisNet, an ablation study is performed in the following ways: i) we remove the flow estimator for alignment, resulting in *w/o flow*, a UNet-like structure that does not perform feature alignment, ii) we replace the gated multiplicative attentive fusion modules with concatenation operations, which is called *w/o att*, iii) we replace the semi-supervised data generation scheme with only the supervised data, which is called *w/o semi*. Table II compares the qualitative scores in terms of SSIM, ms-SSIM, IS and their masked versions. From the table, we observe that the SSIM-based performances substantially deteriorate without the flow-based alignment module. Meanwhile, the gated multiplicative attentive fusion helps to improve the inception scores of the generated images. Also, semi-supervised training improves performance marginally. Visualization is also shown in Fig. 9. From the figure, we observe that our full model is able to retain the global structure due to flow-based alignment. Comparing *w/o att* and *full*, we see that with the gated multiplicative attention module, our model generates globally consistent texture details.
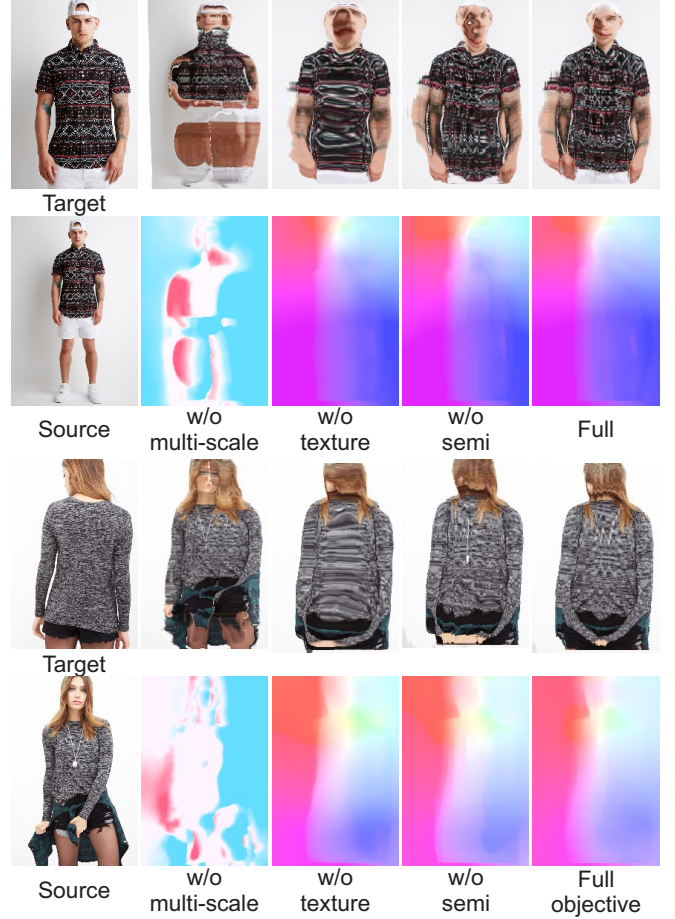

Fig. 8. Comparisons of different unsupervised flow training schemes. Our full flow training objective (Eq. 5) generates more visually plausible and pleasing textures and more consistent flow.

Fig. 9. Visual comparisons of different SynthesisNet training schemes. Our full model generates more visually plausible and pleasing texture details with more coherent global structures.

TABLE II
Quantitative comparison of different flow training schemes and SynthesisNet training schemes in terms of both the masked SSIM/msSSIM/Inception Score (IS) and the Learned Perceptual Image Patch Similarity (LPIPS) at 256×256 and 128×128 resolution. Higher scores are better for metrics with up arrows (↑), and vice versa.

Flow training schemes	SSIM-128↑	msSSIM-128↑	SSIM↑	msSSIM↑	IS-128↑	IS↑	LPIPS↓	LPIPS-128↓
w/o multi-scale	0.822	0.853	0.825	0.839	**4.115 ± 0.211**	**4.689 ± 0.327**	0.240	0.240
w/o texture	**0.837**	0.880	**0.837**	0.861	3.843 ± 0.246	4.204 ± 0.245	0.217	0.217
w/o semi	0.835	0.880	0.834	0.861	3.978 ± 0.348	4.412 ± 0.223	0.196	0.196
full training scheme	0.836	**0.882**	0.835	**0.863**	3.934 ± 0.274	4.404 ± 0.331	**0.193**	**0.193**

SynthesisNet training schemes	SSIM-128↑	msSSIM-128↑	SSIM↑	msSSIM↑	IS-128↑	IS↑	LPIPS↓	LPIPS-128↓
w/o flow	0.849	0.898	0.844	0.877	3.421 ± 0.177	3.952 ± 0.291	0.141	0.141
w/o att	0.853	0.904	0.848	0.883	3.391 ± 0.161	3.946 ± 0.374	0.128	0.128
w/o semi	0.851	0.903	0.846	0.882	3.480 ± 0.273	3.995 ± 0.333	0.128	0.128
full model	**0.854**	**0.905**	**0.848**	**0.884**	**3.540 ± 0.294**	**4.197 ± 0.291**	**0.124**	**0.124**

F. Generalization

To understand the generalization ability of our trained model and how well our model can perform on real-world datasets, we evaluate our trained model on three additional datasets:
Multi-view Clothing dataset The Multi-view Clothing dataset (MVC) [19] contains 161,260 person images and 645,040 pairs in total. We report the results on the MVC dataset using various models that are trained on the DeepFashion dataset. We also report the performance of our finetuned model using 120,000 pairs selected from the MVC training set. Table III shows the evaluation of our approach in comparison to other approaches. The generated new-person images are visualized in Fig. 10.
Amazon Fashion Video Data We evaluate our approach on a set of online video data. Specifically, we crawl clothing item demo videos from the Amazon Fashion website. The initial frame from various source video is used as the source images to synthesize each frame from the target video. The synthesized videos are shown in the supplementary materials. In Fig. 11, the top row shows the target video, while the resting rows show the synthesized video with different clothing styles from source images. As demonstrated in Fig. 11, our approach generates temporal-consistent frames with distinctive texture details, suggesting that our method can effectively generalize to unseen poses and clothing styles.
Garment transfer to real person To examine the applicability of our approach in real-world scenes, we collect videos of people in real scenes with various poses using a typical smartphone. Fig. 12 visualizes consecutive frames of our captured video and our transferred video, showing that our approach can generate visually plausible and pleasing new clothing styles under challenging real-world environments.

V. Conclusion

To better model person appearance transformation for pose-guided synthesis, we propose an unsupervised pose flow learning scheme that learns to transfer appearance from target images. Furthermore, we propose a texture preserving objective and an augmentation-based self-supervision scheme which are shown to be effective for learning appearance-preserving pose flow. Based on the learned pose flow, we propose a coarse-to-fine synthesis pipeline using a carefully designed network structure for multi-scale feature domain alignment.

To address the misalignment issue, we propose a gated multiplicative attention module. In addition, masking layers are used to preserve target identities and background information. Experiments on the DeepFasion, MVC, and other real-world datasets have validated the effectiveness and robustness of our approach.

Appendix A
Adaptation of FlowNetS

To implement the flow estimator function $\text{Flow}()$ from Eq. 1, we use the FlowNetS network structure. However, several adaptations are made. First, we reduce the channel of each convolution/deconvolution layer to 64 for memory efficiency. Second, to improve the flow definition at scale 0, the $\times 4$ bilinear upsampling layer at the end of the original FlowNetS is replaced by two $\times 2$ U-Net upsampling modules.

Appendix B
Code for gated multiplicative attention filtering

We show that the gated multiplicative attention filtering

$$\mathbf{f}_{s \to t}^{(l)'} = \mathbf{f}_{s \to t}^{(l)} \odot \sigma(\mathbf{f}_{s \to t}^{(l)\top} \mathbf{W}^{(l)} \mathbf{f}_t^{(l)}),$$

from Eq. 11 can be implemented using 3 lines of code in PyTorch:

Algorithm 1 Gated multiplicative attention filtering

Input: $\mathbf{f}_{s \to t}^{(l)'}, \mathbf{f}_t^{(l)}$
Output: $\mathbf{f}_{s \to t}^{(l)'}$
    compute filter $\sigma(\mathbf{f}_{s \to t}^{(l)\top} \mathbf{W}^{(l)} \mathbf{f}_t^{(l)})$:
1: `att = torch.sum(conv_W(`$\mathbf{f}_{s \to t}^{(l)}$`) *`$\mathbf{f}_t^{(l)}$`, 1)`
2: `att = torch.sigmoid(att)`
    perform filtering :
3: $\mathbf{f}_{s \to t}^{(l)'}$ `= torch.mul(`$\mathbf{f}_{s \to t}^{(l)}$`, att)`
4: **return** $\mathbf{f}_{s \to t}^{(l)'}$

---

where function `conv_W()` defines a 1×1 convolutional operation with its trainable parameters $\mathbf{W}^{(l)}$.

TABLE III
QUANTITATIVE COMPARISON OF VARIOUS APPROACHES ON THE MVC DATASET USING THE MODELS TRAINED ON THE DEEPFASHION DATASET. PERFORMANCES ARE MEASURED IN TERMS OF THE MASKED SSIM/MSSSIM/IS SCORES AT 256×256 RESOLUTION AND 128×128 RESOLUTION. HIGHER SCORES ARE BETTER FOR METRICS WITH UP ARROWS (↑), AND VICE VERSA. TOP TWO SCORES ARE IN BOLD.

Methods	SSIM↑	SSIM-128↑	msSSIM↑	msSSIM-128↑	IS↑	IS-128↑
PG2 [22]	0.817	0.806	0.851	0.840	3.401 ± 0.269	3.662 ± 0.361
BodyROI7 [23]	0.798	0.792	0.828	0.823	3.043 ± 0.250	3.039 ± 0.152
DSCF [34]	0.816	0.810	0.846	0.841	3.358 ± 0.229	3.151 ± 0.229
Vunet [4]	0.806	0.794	0.840	0.833	3.294 ± 0.190	2.871 ± 0.222
Ours	**0.836**	**0.839**	**0.857**	**0.853**	**3.603 ± 0.300**	**3.451 ± 0.426**
Ours-Finetuned	**0.839**	**0.840**	**0.863**	**0.859**	**3.737 ± 0.415**	**3.365 ± 0.273**

Fig. 10. Comparison with the state-of-the-art approaches on the MVC dataset. Patches are zoomed in to visualize detailed textures. The last two columns depict our DeepFashion trained model and our MVC finetuned model.

REFERENCES

[1] R. Alp Güler, N. Neverova, and I. Kokkinos. Densepose: Dense human pose estimation in the wild. In *Proceedings of the IEEE Conference on Computer Vision and Pattern Recognition*, pages 7297–7306, 2018.

[2] Q. Chen and V. Koltun. Photographic image synthesis with cascaded refinement networks. In *Proceedings of the IEEE International Conference on Computer Vision*, pages 1511–1520, 2017.

[3] H. Dong, X. Liang, K. Gong, H. Lai, J. Zhu, and J. Yin. Soft-gated warping-gan for pose-guided person image synthesis. In *Advances in Neural Information Processing Systems*, pages 472–482, 2018.

[4] P. Esser, E. Sutter, and B. Ommer. A variational u-net for conditional appearance and shape generation. 2018.

[5] P. Fischer, A. Dosovitskiy, E. Ilg, P. Häusser, C. Hazırbaş, V. Golkov, P. Van der Smagt, D. Cremers, and T. Brox. Flownet: Learning optical flow with convolutional networks. *arXiv preprint arXiv:1504.06852*, 2015.

[6] L. Gatys, A. S. Ecker, and M. Bethge. Texture synthesis using convolutional neural networks. In *Advances in neural information processing systems*, pages 262–270, 2015.

[7] K. Gong, X. Liang, D. Zhang, X. Shen, and L. Lin. Look into person: Self-supervised structure-sensitive learning and a new benchmark for human parsing. In *Proceedings of the IEEE Conference on Computer Vision and Pattern Recognition*, pages 932–940, 2017.

[8] I. Goodfellow, J. Pouget-Abadie, M. Mirza, B. Xu, D. Warde-Farley, S. Ozair, A. Courville, and Y. Bengio. Generative adversarial nets. In *Advances in neural information processing systems*, pages 2672–2680, 2014.

[9] I. Gulrajani, F. Ahmed, M. Arjovsky, V. Dumoulin, and A. C. Courville. Improved training of wasserstein gans. In *Advances in Neural Information Processing Systems*, pages 5767–5777, 2017.

[10] X. Han, Z. Wu, Z. Wu, R. Yu, and L. S. Davis. Viton: An image-based virtual try-on network. In *Proceedings of the IEEE Conference on Computer Vision and Pattern Recognition*, pages 7543–7552, 2018.

[11] P. Isola, J.-Y. Zhu, T. Zhou, and A. A. Efros. Image-to-image translation with conditional adversarial networks. In *Proceedings of the IEEE conference on computer vision and pattern recognition*, pages 1125–1134, 2017.

[12] M. Jaderberg, K. Simonyan, A. Zisserman, et al. Spatial transformer networks. In *Advances in neural information processing systems*, pages 2017–2025, 2015.

[13] J. Y. Jason, A. W. Harley, and K. G. Derpanis. Back to basics: Unsupervised learning of optical flow via brightness constancy and motion smoothness. In *European Conference on Computer Vision*, pages 3–10. Springer, 2016.

[14] J. Johnson, A. Alahi, and L. Fei-Fei. Perceptual losses for real-time style transfer and super-resolution. In *ECCV*, pages 694–711. Springer, 2016.

[15] D. P. Kingma and J. Ba. Adam: A method for stochastic optimization. *arXiv preprint arXiv:1412.6980*, 2014.

[16] D. P. Kingma and M. Welling. Auto-encoding variational bayes. *arXiv preprint arXiv:1312.6114*, 2013.

[17] C. Li and M. Wand. Precomputed real-time texture synthesis with markovian generative adversarial networks. In *European Conference on Computer Vision*, pages 702–716. Springer, 2016.
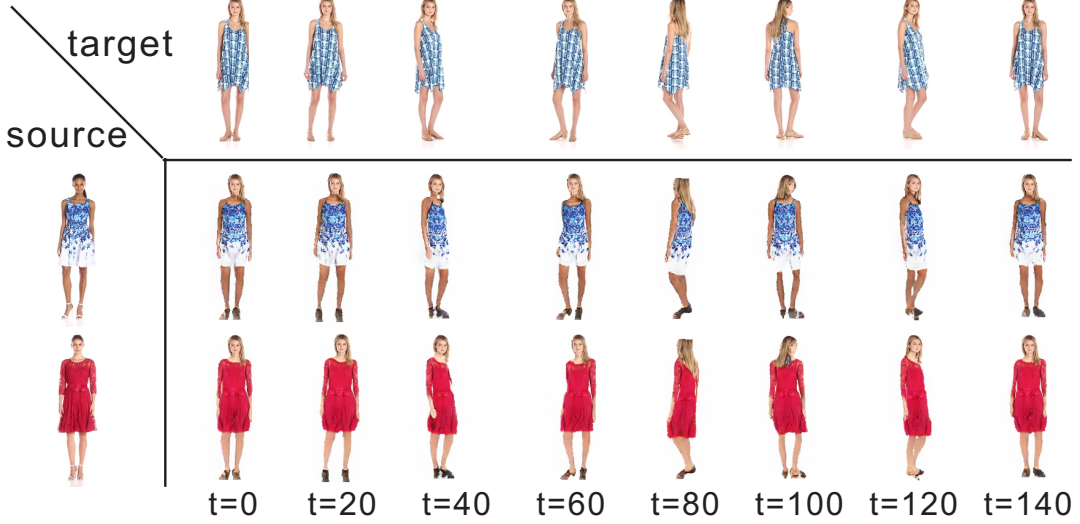
Fig. 11. Garment transfer on the Amazon Fashion videos. The top row shows the target frames, while the resting rows show the synthesized frames. The horizontal axis represents the time step. Our approach can generate temporally consistent frames with distinctive texture details.
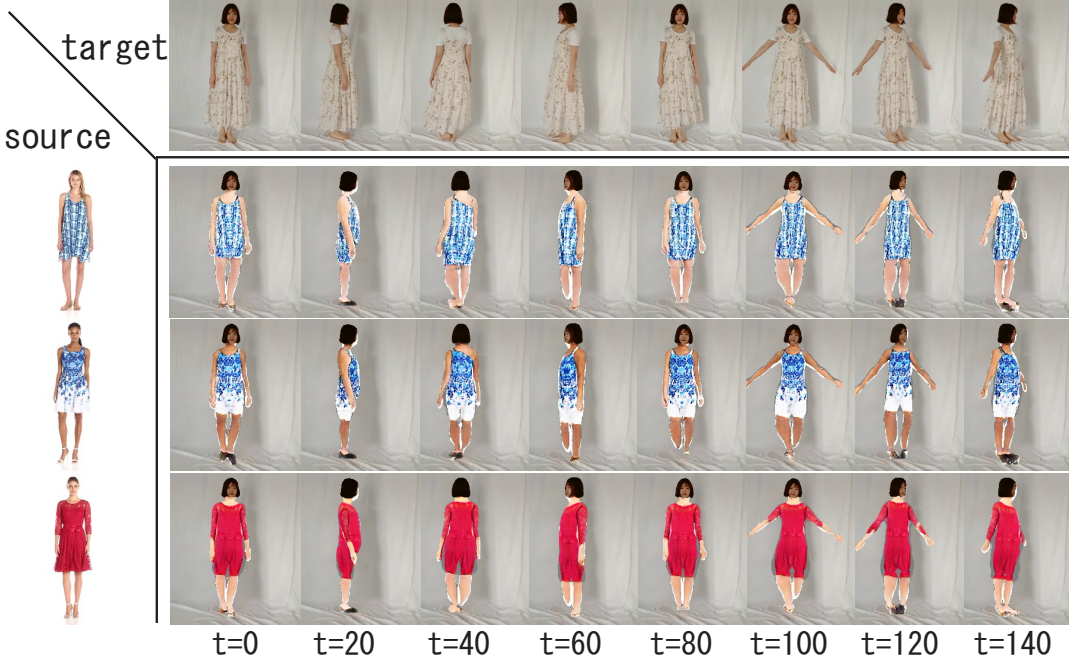

Fig. 12. Garment transfer on our self-collected real-world videos. The top row shows the target frames, while the remaining rows show the synthesized frames. The horizontal axis represents the time step. Our approach can generate temporally consistent frames with distinctive texture details.

[18] Y. Li, C. Huang, and C. C. Loy. Dense intrinsic appearance flow for human pose transfer. In *IEEE Conference on Computer Vision and Pattern Recognition*, 2019.

[19] K.-H. Liu, T.-Y. Chen, and C.-S. Chen. Mvc: A dataset for view-invariant clothing retrieval and attribute prediction. In *Proceedings of the 2016 ACM on International Conference on Multimedia Retrieval*, pages 313–316. ACM, 2016.

[20] Z. Liu, P. Luo, S. Qiu, X. Wang, and X. Tang. Deepfashion: Powering robust clothes recognition and retrieval with rich annotations. In *Proceedings of the IEEE conference on computer vision and pattern recognition*, pages 1096–1104, 2016.

[21] M. Loper, N. Mahmood, J. Romero, G. Pons-Moll, and M. J. Black. SMPL: A skinned multi-person linear model. *ACM Trans. Graphics (Proc. SIGGRAPH Asia)*, 34(6):248:1–248:16, Oct. 2015.

[22] L. Ma, X. Jia, Q. Sun, B. Schiele, T. Tuytelaars, and L. Van Gool. Pose guided person image generation. In *Advances in Neural Information Processing Systems*, pages 406–416, 2017.

[23] L. Ma, Q. Sun, S. Georgoulis, L. Van Gool, B. Schiele, and M. Fritz. Disentangled person image generation. In *Proceedings of the IEEE Conference on Computer Vision and Pattern Recognition*, pages 99–108, 2018.

[24] X. Mao, Q. Li, H. Xie, R. Y. Lau, Z. Wang, and S. Paul Smolley. Least squares generative adversarial networks. In *Proceedings of the IEEE International Conference on Computer Vision*, pages 2794–2802, 2017.

[25] S. Meister, J. Hur, and S. Roth. Unflow: Unsupervised learning of optical flow with a bidirectional census loss. In *Thirty-Second AAAI Conference on Artificial Intelligence*, 2018.

[26] M. Mirza and S. Osindero. Conditional generative adversarial nets. *arXiv preprint arXiv:1411.1784*, 2014.

[27] T. Miyato, T. Kataoka, M. Koyama, and Y. Yoshida. Spectral normalization for generative adversarial networks. *arXiv preprint*

arXiv:1802.05957, 2018.

[28] N. Neverova, R. Alp Guler, and I. Kokkinos. Dense pose transfer. In *Proceedings of the European Conference on Computer Vision (ECCV)*, pages 123–138, 2018.

[29] A. Raj, P. Sangkloy, H. Chang, J. Hays, D. Ceylan, and J. Lu. Swapnet: Image based garment transfer. In *European Conference on Computer Vision*, pages 679–695. Springer, 2018.

[30] Z. Ren, J. Yan, B. Ni, B. Liu, X. Yang, and H. Zha. Unsupervised deep learning for optical flow estimation. In *Thirty-First AAAI Conference on Artificial Intelligence*, 2017.

[31] I. Rocco, R. Arandjelovic, and J. Sivic. Convolutional neural network architecture for geometric matching. In *Proceedings of the IEEE Conference on Computer Vision and Pattern Recognition*, pages 6148–6157, 2017.

[32] O. Ronneberger, P. Fischer, and T. Brox. U-net: Convolutional networks for biomedical image segmentation. In *International Conference on Medical image computing and computer-assisted intervention*, pages 234–241. Springer, 2015.

[33] T. Salimans, I. Goodfellow, W. Zaremba, V. Cheung, A. Radford, and X. Chen. Improved techniques for training gans. In *Advances in neural information processing systems*, pages 2234–2242, 2016.

[34] A. Siarohin, E. Sangineto, S. Lathuilière, and N. Sebe. Deformable gans for pose-based human image generation. In *Proceedings of the IEEE Conference on Computer Vision and Pattern Recognition*, pages 3408–3416, 2018.

[35] K. Simonyan and A. Zisserman. Very deep convolutional networks for large-scale image recognition. *arXiv preprint arXiv:1409.1556*, 2014.

[36] D. Sun, S. Roth, and M. J. Black. Secrets of optical flow estimation and their principles. In *2010 IEEE computer society conference on computer vision and pattern recognition*, pages 2432–2439. IEEE, 2010.

[37] B. Wang, H. Zheng, X. Liang, Y. Chen, L. Lin, and M. Yang. Toward characteristic-preserving image-based virtual try-on network. In *Proceedings of the European Conference on Computer Vision (ECCV)*, pages 589–604, 2018.

[38] T.-C. Wang, M.-Y. Liu, J.-Y. Zhu, A. Tao, J. Kautz, and B. Catanzaro. High-resolution image synthesis and semantic manipulation with conditional gans. In *Proceedings of the IEEE Conference on Computer Vision and Pattern Recognition*, pages 8798–8807, 2018.

[39] Y. Wang, Y. Yang, Z. Yang, L. Zhao, P. Wang, and W. Xu. Occlusion aware unsupervised learning of optical flow. In *Proceedings of the IEEE Conference on Computer Vision and Pattern Recognition*, pages 4884–4893, 2018.

[40] Z. Wang, A. C. Bovik, H. R. Sheikh, and E. P. Simoncelli. Image quality assessment: from error visibility to structural similarity. *IEEE transactions on image processing*, 13(4):600–612, 2004.

[41] Z. Wang, E. P. Simoncelli, and A. C. Bovik. Multiscale structural similarity for image quality assessment. In *The Thrity-Seventh Asilomar Conference on Signals, Systems & Computers, 2003*, volume 2, pages 1398–1402. Ieee, 2003.

[42] Z. Wu, G. Lin, Q. Tao, and J. Cai. M2e-try on net: Fashion from model to everyone. *arXiv preprint arXiv:1811.08599*, 2018.

[43] L. Xu, Y. Liu, W. Cheng, K. Guo, G. Zhou, Q. Dai, and L. Fang. Flycap: Markerless motion capture using multiple autonomous flying cameras. *IEEE transactions on visualization and computer graphics*, 2017.

[44] H. Zhang, T. Xu, H. Li, S. Zhang, X. Wang, X. Huang, and D. N. Metaxas. Stackgan: Text to photo-realistic image synthesis with stacked generative adversarial networks. In *Proceedings of the IEEE International Conference on Computer Vision*, pages 5907–5915, 2017.

[45] R. Zhang, P. Isola, A. A. Efros, E. Shechtman, and O. Wang. The unreasonable effectiveness of deep features as a perceptual metric. In *Proceedings of the IEEE Conference on Computer Vision and Pattern Recognition*, pages 586–595, 2018.

[46] J.-Y. Zhu, T. Park, P. Isola, and A. A. Efros. Unpaired image-to-image translation using cycle-consistent adversarial networks. In *Proceedings of the IEEE International Conference on Computer Vision*, pages 2223–2232, 2017.

Haitian Zheng Haitian Zheng received the B.Sc. and the M.Sc. degrees in electronics engineering and informatics science from the University of Science and Technology of China, under the supervision of Prof. Lu Fang, in 2012 and 2016, respectively. He is currently pursuing the PhD degree with the Computer Science Department, University of Rochester, under the supervision of Prof. Jiebo Luo. His research interests include computer vision and machine learning.

Lele Chen Lele is a Ph.D candidate advised by Prof. Chenliang Xu in URCS. He received his M.S. degree in Computer Science from University of Rochester in 2018 and B.S. degree in Computer Science from Donghua University in 2016. His research interests are multimodal modeling and video object detection/segmentation.

Chenliang Xu Chenliang Xu is an Assistant Professor in the Department of Computer Science at the University of Rochester. He received his Ph.D. degree from the University of Michigan in 2016, the MS degree from SUNY Buffalo in 2012, both in Computer Science, and the BS degree in Information and Computing Science from Nanjing University of Aeronautics and Astronautics in 2010. He is the recipient of multiple NSF awards including BIG-DATA 2017, CDS&E 2018, and IIS Core 2018, the University of Rochester AR/VR Pilot Award 2017, Tencent Rhino-Bird Award 2018, the Best Paper Award at Sound and Music Computing 2017, and an Open Source Code Award in CVPR 2012. Xu has authored more than 30 peer-reviewed papers in venues such as IJCV, CVPR, ICCV, ECCV, IJCAI, and AAAI on topics of his research interest including computer vision and its relations to natural language, robotics, and data science. He co-organized the CVPR 2017 Workshop on video understanding and has served as a PC member and a regular reviewer for various international conferences and journals.

Jiebo Luo Jiebo Luo (S93, M96, SM99, F09) joined the Department of Computer Science at the University of Rochester in 2011, after a prolific career of over 15 years with Kodak Research. He has authored over 400 technical papers and holds over 90 U.S. patents. His research interests include computer vision, machine learning, data mining, social media,and biomedical informatics. He has served as the Program Chair of the ACM Multimedia 2010, IEEE CVPR 2012, ACM ICMR 2016, and IEEE ICIP 2017, and on the Editorial Boards of the IEEE TRANSACTIONS ON PATTERN ANALYSIS AND MACHINE IN-TELLIGENCE, IEEE TRANSACTIONS ON MULTIMEDIA, IEEE TRANS-ACTIONS ON CIRCUITS AND SYSTEMS FOR VIDEO TECHNOLOGY, IEEE TRANSACTIONS ON BIG DATA, Pattern Recognition, Machine Vision and Applications, and ACM Transactions on Intelligent Systems and Technology. He is also a Fellow of ACM, AAAI, SPIE and IAPR.